Progress In Electromagnetics Research M, Vol. 63, 131–139, 2018

Investigation of Fold-Dependent Behavior in an Origami-Inspired FSS under Normal Incidence

Deanna Sessions[1, 2, 3, *], Kazuko Fuchi[4], Sumana Pallampati[1], David Grayson[1], Steven Seiler[2, 3], Giorgio Bazzan[2, 3], Gregory Reich[5], Philip Buskohl[2], and Gregory Huff[1, 3]

Abstract—Frequency selective surfaces (FSS) filter specific electromagnetic (EM) frequencies defined by the geometry and often fixed periodic spacing of a conductive element array. By embedding the FSS pattern into an origami structure, we expand the number of physical configurations and periodicities of the FSS, allowing for fold-driven frequency tuning. The goal of this work is to examine the fold-dependent polarization and frequency behavior of an origami-inspired FSS under normal incidence and provide physical insight into its performance. The FSS is tessellated with the Miura-ori pattern and uses resonant length metallic dipoles with orthogonal orientations for two primary modes of polarization. A driven dipole model with geometric morphologies, representative of the folding operations, provides physical insight into the observed behavior of the FSS. Full-wave simulations and experimental results demonstrate a shift in resonant frequency and transmissivity with folding, highlighting the potential of origami structures as an underlying mechanism to achieve fold-driven EM agility in FSSs.

1. INTRODUCTION

Origami inspired folding concepts have been adopted in many engineering applications, including solar arrays [1, 2], optical systems [3], and antennas [4–8]. In addition, origami-inspired frequency selective surfaces (FSS) have been explored using linearly polarized elements that allowed for frequency tuning at multiple angles of oblique incidence [9]. This inspired the exploration of a large variety of origami FSSs through simulations utilizing the combination of origami mathematics and conductive trace drawing based on a mapping function [10]. Current interest is fueled in part by recent developments in origami mathematics [11]. This mathematical treatment has provided computational origami design tools that have accelerated the use of origami folding concepts by linking geometric [12, 13], structural [14, 15] and, more recently, electromagnetic (EM) design criteria [16]. This link to structural engineering has brought interest to incorporating electromagnetic properties into structures that undergo deployment or morphing through an origami-like motion for various targets including compact packaging, vibration suppression and aerodynamic control. While these structures can achieve desired physical reconfiguration through a proper placement of actuators, most do not possess electromagnetic reconfiguration abilities. The incorporation of origami with electromagnetic capabilities into these structures builds upon physical systems that already exist in a way that imposes additional functionalities.

One of the key features arising from the origami-inspired physical reconfiguration of antennas, FSS, and other passive structures has been in the ability to engineer EM agility into their operation.

Received 25 September 2017, Accepted 1 December 2017, Scheduled 11 January 2018
* Corresponding author: Deanna Sessions (deanna.sessions@tamu.edu).
[1] Texas A&M University, Department of Electrical & Computer Engineering, College Station, TX 77843, USA. [2] Air Force Research Laboratory, Materials & Manufacturing Directorate, Wright Patterson AFB, OH 45433, USA. [3] UES Inc, Beavercreek, OH 45432, USA. [4] University of Dayton Research Institute, Dayton, OH 45469, USA. [5] Air Force Research Laboratory, Aerospace Systems Directorate, Wright Patterson AFB, OH 45433, USA.

Reconfiguration is traditionally achieved by implementing lumped components that are electrically adjusted or the physical movement of electromagnetic components in space; origami patterns lend well to a geometrically defined problem space for spatial movement. Examples of origami-inspired reconfiguration include frequency tunability using helical antennas [6] printed on origami-inspired spring structures and the folding of an FSS in the Miura-ori pattern with elements located on the facets [9]. These and other examples have illustrated the potential for unique RF capabilities through the adoption of origami design principles, but they also showcase a spectrum of design challenges that have emerged.

For in-service folding of an FSS, the primary challenge is enabling predictive EM capabilities throughout folding. This requires linking the relationships between FSS topology and the origami folding operations. Establishing this connection between EM agility and folding requires an understanding of the impact from symmetry, tiling, and the EM properties. It also relies on structural, material, and mechanical constraints. The goal of this work is to present a systematic investigation of the potential for in-service tuning of an origami-inspired folding stop-band FSS. To facilitate the experimental verification, the fabrication process incorporates a laser cut polypropylene substrate with precision cut copper tape as the RF components. This will act as a basis for additional investigations in both the simulation and experimentation of various origami-inspired EM designs. For this work, the topology and folding behavior are discussed first. Simulations of a driven element model are then presented to provide some physical insight into the EM performance of the folding structure. Simulated and experimental results for both a flat and intermediate folded state follow this. A brief summary concludes the work.

2. ORIGAMI INSPIRED FSS DESIGN

The origami-inspired FSS (Fig. 1(a)) merges the Miura-ori tessellation *Tile 1* (Fig. 1(b)) with the FSS unit cell *Tile 2* (Fig. 1(c)). The facets of *Tile 1* are defined by parallelograms with a vertex angle $\alpha = 45°$, base $L = 80\,\text{mm}$, and height $0.5L$. *Tile 2* is a square with side lengths L and four rotationally symmetric resonant-length metallic strips of length $l = 38\,\text{mm}$, width $W = 3\,\text{mm}$, and edge-spacing $d = 10\,\text{mm}$. The metallic strips are supported by a 0.75 mm thick polypropylene substrate with $\epsilon_r = 2.2$, $\tan\delta = 0.01$.

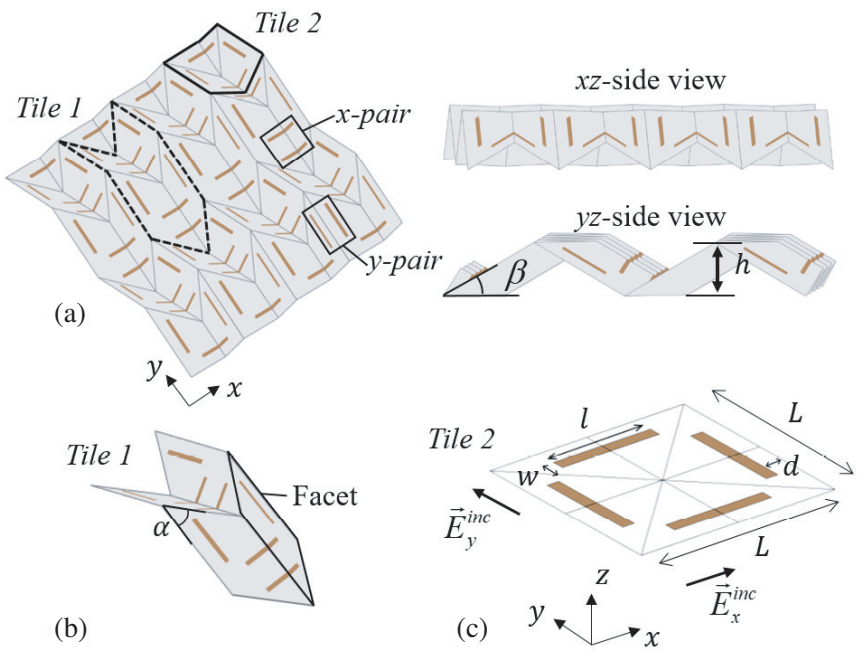

Figure 1. (a) Origami-inspired foldable FSS, (b) Miura-ori tessellation *Tile 1* representing the tiling unit of the fold pattern and (c) *Tile 2* representing the unit cell of the FSS.

The Miura-ori folding of the FSS in this work is parameterized analytically [9], but rigid origami simulation [13] and mechanical analysis [14] exist. It is summarized by considering two rotational operations on each of the four parallelogram facets in *Tile 1*. The lower right facet is first rotated by the angle β about the x-axis; β is the parameter used to describe the extent of folding. A rotation of the facet about the z-axis through the angle $\gamma = \tan^{-1}(\cot\alpha/\cos\beta)$ follows this. The reflected nature of the symmetry of *Tile 1* can then be used to calculate the orientations of the other facets. The resulting FSS is symmetric with $\beta = 0°$ (flat), but symmetry is broken when the FSS is folded; so *Tile 1* serves as the foldable periodic unit cell of the FSS. Geometrically, it has an equivalent area and the same number of metallic strips as two copies of *Tile 2*.

3. PHYSICAL RECONFIGURATION

The metallic strips within the FSS are subjected to two unique fold-induced changes in symmetry, shape, and spacing based on their placement in *Tile 2*. The geometric impact of folding is considered first using a pair of driven elements as a surrogate to isolate the primary mechanisms of EM tuning.

3.1. Folding and Symmetry

The FSS unit cell (*Tile 2*) and Miura-ori tessellation (*Tile 1*) generate closely-spaced pairs of co-linear metallic strips with two orthogonal orientations (Fig. 1(a)). The *x-pair* strips remain aligned with the x-axis and the *y-pair* strips remain aligned with the y-axis throughout folding. Each undergoes a unique physical reconfiguration. The *x-pairs* are bisected by valley and mountain folds in the y-dir. such that they fold across these creases by the angle β but their pair-wise separation $2d$ remains unchanged. The *y-pairs* are positioned on facets, so they remain physically unchanged and co-linear throughout folding, but they experience mirror symmetry, so they are rotated by β, and their separation decreases by $2d\sin\beta$ (see Fig. 2).

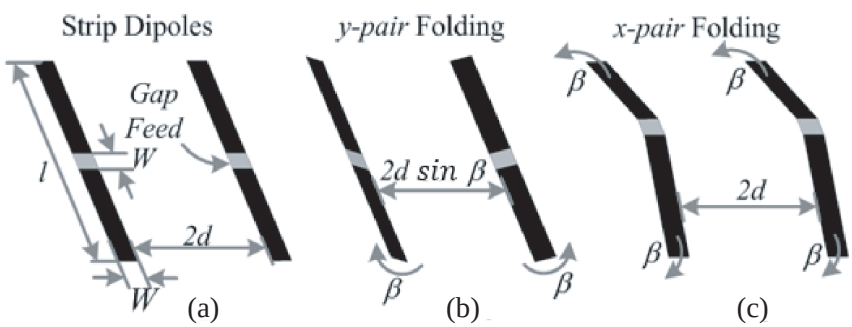

Figure 2. (a) Gap fed (driven) pair of strip dipoles representing the flat ($\beta = 0°$) and the folding motion of (b) y-pairs and (c) x-pairs in the origami-inspired foldable FSS.

3.2. Polarization-Dependent Frequency Agility

The physical reconfiguration of x- and *y-pairs* is proposed as the dominant physical mechanism giving rise to the fold-dependent polarization and frequency agility. Other changes in morphology clearly influence the stop-band characteristics, including the changing distance between x- and *y-pairs*, but for the shallow bend angles $0° \leq \beta \leq 40°$ these and other mechanisms are considered as secondary effects. Under these assumptions, the dominant reconfiguration mechanism is isolated using two normally-incident linearly-polarized plane waves $\vec{E}_x^{inc} = \hat{x}E_0e^{-jkz}$ (*x-pol.*) and $\vec{E}_y^{inc} = \hat{y}E_0e^{-jkz}$ (*y-pol.*), which are aligned to the x- and *y-pairs*, respectively.

Simulations [17] of gap-fed co-linear dipole pairs (Fig. 2(a)) undergoing physical reconfiguration representative of x- and *y-pairs* in the FSS have been performed. This is intended to provide some basic physical insight into the impact of folding in the FSS. The impedance match of the elements is

proposed to serve as a performance metric for this purpose. The pairs are examined in isolation, so their response will only provide insight into major performance trends as they relate to the resonant properties of the elements.

Figures 3 and 4 show the magnitudes of the input reflection coefficient $|S_{11}|$ in dB (source impedance of $Z_0 = 73\,\Omega$) for the *x*- and *y-pair* folding behaviors, respectively. These simulations examine the behavior over the S-band (2.8 GHz to 4 GHz). They do not include dielectric loading from the substrate, any capacitive loading arising from the W-by-W gap feed, or coupling to the nearest neighbor that the elements experience in the FSS lattice. Without the placement of the element in the

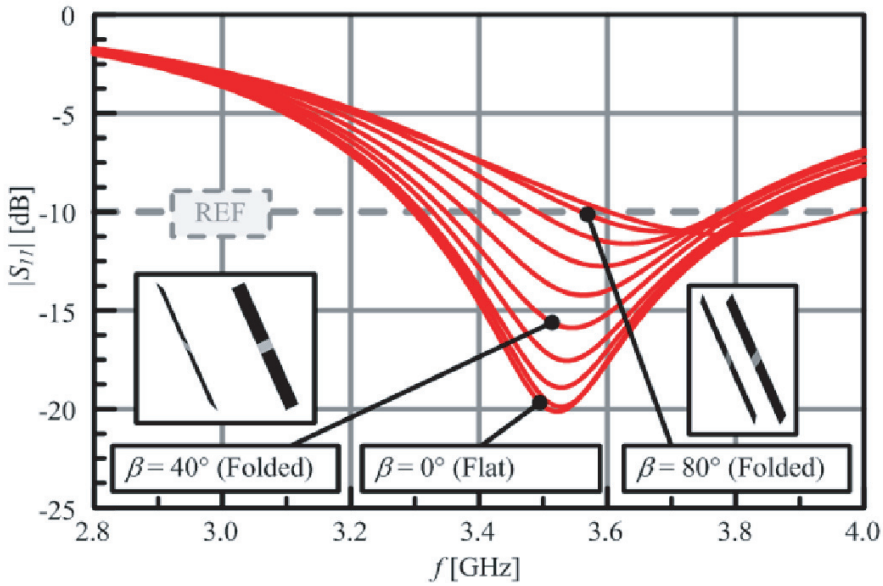

Figure 3. Simulation input reflection coefficient $|S_{11}|$ in dB of coupled dipoles undergoing *y-pair* physical reconfiguration for $0° \leq \beta \leq 90°$ in 10° increments.

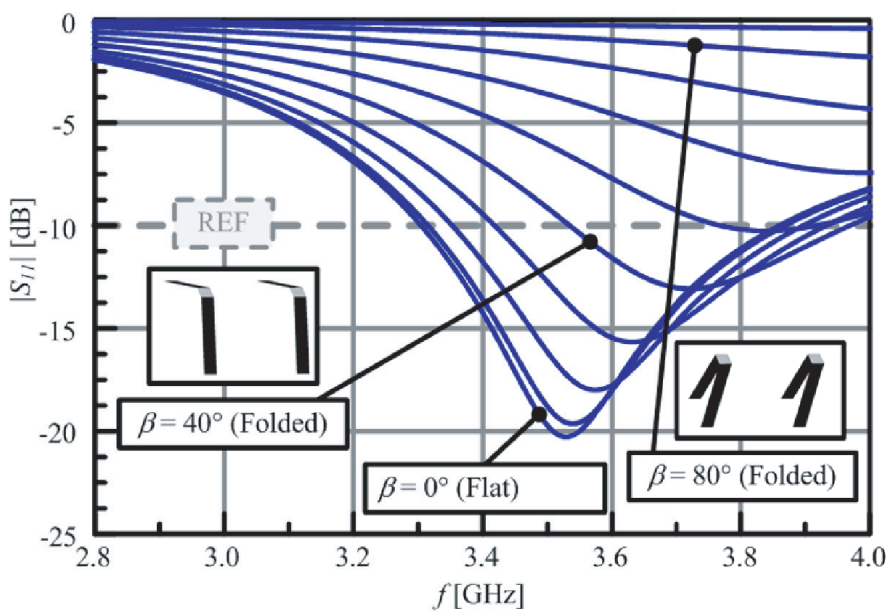

Figure 4. Simulation input reflection coefficient $|S_{11}|$ in dB of coupled dipoles undergoing *x-pair* physical reconfiguration for $0° \leq \beta \leq 90°$ in 10° increments.

lattice to provide proper loading, a response with a shift in frequency is expected based primarily on the lack of capacitance in the model. However, provided that the impedance match serves as an indicator of stop-band behavior in the FSS, these simulations indicate that the two polarizations will experience in-service fold-driven frequency agility in the stop-band filtering behavior of the FSS.

The most notable observations are the upward shift in the center-frequency and a broadening of the matched impedance bandwidth as β is increased. In the *y-pairs* the impact of folding is less pronounced, but the elements clearly detune. This is attributed to mutual coupling as the distance between the two co-linear dipoles is reduced. For the *x-pairs* the impact is more pronounced and attributed to the physical folding of the dipoles which results in parallel-strip transmission lines terminated in open circuits. These results indicate that the orientation and placement of the elements in the FSS will directly impact the aggregate stop-band behavior and create polarization-dependent frequency agility.

3.3. FSS Simulation

Full-wave EM simulations [17] of *Tile 1* are performed to examine the performance of the FSS in the S-band as a function of bend angle. The computational domain is extended in the vertical direction above and below the origami sheet and perfectly matched layers are used at the input and output ports. Periodic boundaries are applied to the six-side walls, and normally incident plane wave excitations are carried out independently for chosen bend angles.

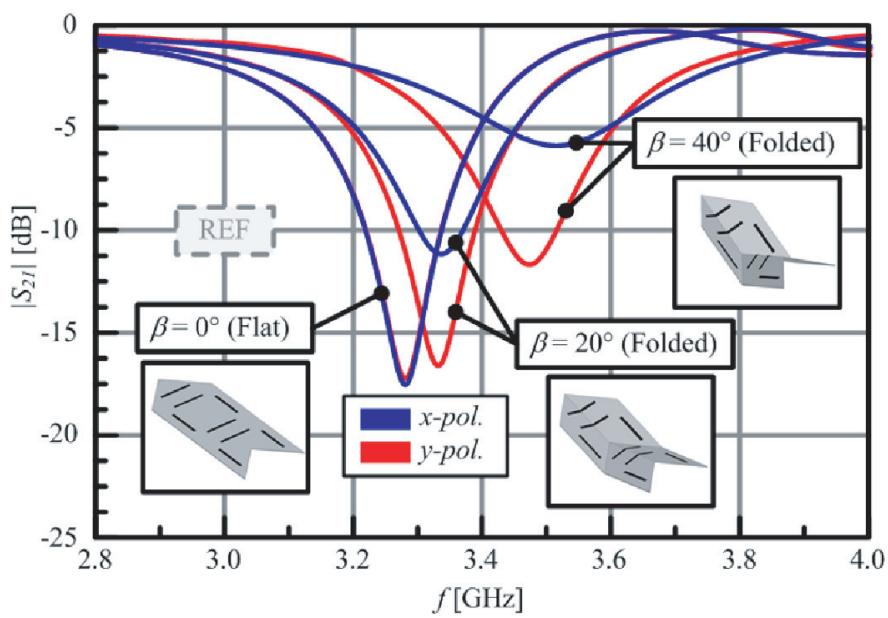

Figure 5. Simulated transmission coefficient (S_{21}) of origami-inspired FSS in flat ($\beta = 0°$) and folded ($\beta = 20°$ and $40°$) states for both polarizations.

Figure 5 shows a subset of results including the flat ($\beta = 0°$) and two-folded ($\beta = 20°$ and $40°$) states. Both the *x-* and *y-pairs* follow the general trends observed in folding dipole simulations using *x-pol.* and *y-pol.* excitations, respectively. This includes the upward shift in the center of the stop-band and a corresponding decrease in the -10 dB bandwidth of the stop-band. One of the primary differences observed in the full wave simulation of *Tile 1* resides in the degree of EM agility achieved from folding. In both polarizations, the agility is less pronounced; the foldable FSS under the *x-pol.* excitation is operational only up to the $\beta = 20°$ state. This behavior is attributed to contributions from higher-order effects in the lattice not accounted for in the simplistic driven dipole model, as well as secondary geometry effects that produce slight differentials in the z-direction, (i.e., tilt and shift). Isolating all of these effects in relation to the EM properties require a sophisticated model that is capable of toggling the individual factors and is currently under investigation. Despite these combined complex effects, both of the polarizations maintain the same relative frequency tuning dependency when folded.

4. EXPERIMENT

4.1. Fabrication

Four 32 cm-by-32 cm polypropylene sheets were laser machined utilizing a 10.6 μm wavelength CO_2 laser to score the fold lines of the Miura-ori tessellation. After scoring the pattern the sheet was populated with metallic strips made from precision-cut copper tape. An 8×8 array of *Tile 2* dipole patterns were assembled using masking tape from a set of four 4×4 arrays. Fig. 6 shows the FSS in the flat and folded states.

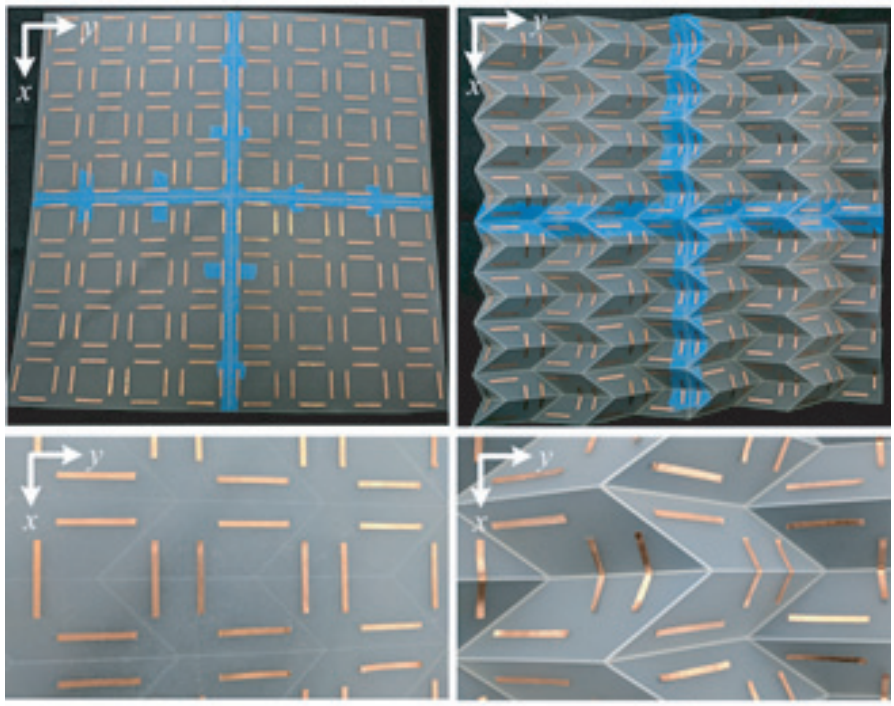

(a) (b)

Figure 6. (a) Flat and (b) folded states of the fabricated origami-inspired FSS.

4.2. Measurement

Figure 7 shows the measurement setup, which includes two S-band pyramidal horn antennas spaced approximately 2.9 m apart with the FSS suspended at the midpoint. A short-open-load-thru (SOLT) calibration was performed first over a frequency range of 2.8 GHz to 4.4 GHz. A reflective 2.54 mm thick aluminum sheet is then positioned in place of the FSS and a time domain transformation is performed to locate the plane of the FSS in the time domain (9.66 ns in this experiment).

A gated-reflect-line (GRL) calibration is then used to shift the reference plane onto the surface of the FSS by measuring a reflect standard (aluminum sheet) and a free-space thru standard. A 5 ns time gate is placed around the reference plane to filter out unwanted reflected signals from interfering objects. The FSS is measured at the reference plane in both horizontal (*x-pol.*) and vertical (*y-pol.*) orientations and the height is adjusted such that the center of the FSS is aligned with the line of sight of the antennas.

Figure 8 shows the simulated and measured magnitudes of the transmission coefficient $\mid S_{21} \mid$ in dB for the flat ($\beta = 0°$) and folded ($\beta = 36.8°$) fabricated FSS. The fold angle was calculated analytically by measuring the height of the fabricated folded structure. The measured performance of the fabricated FSS generally follows the response predicted by simulation for the unfolded state and at the calculated angle of the fabricated sample. The fabricated structures have a lower Q in both polarizations and

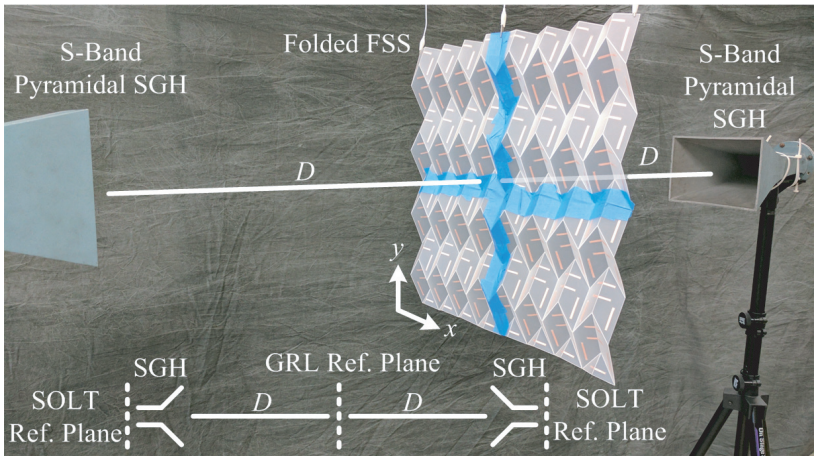

Figure 7. Experimental setup used for the measurement of the origami-inspired FSS and diagram of calibration planes.

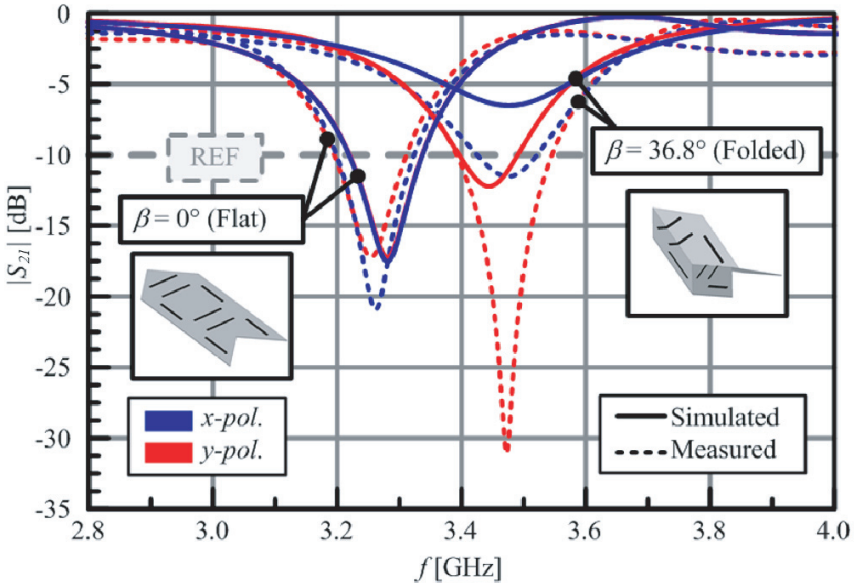

Figure 8. Simulated (solid) and measured (dashed) transmission coefficient ($|\ S_{21}\ |$ in dB) of the origami-inspired FSS in flat ($\beta = 0°$) and folded ($\beta = 36.8°$) states.

in both bend angles. This artifact of measurement is more pronounced in the folded structure, and attributed to calibration limitations in time gating arising from the folded structure extending beyond the reference planes due to the deviation from the reference plane in the measurement setup. This implies that the measured stop-band performance is exaggerated, and the folded FSS only provides a marginal filtering capability in the x-pol at a fold angle of 36.8°. Provided that this discrepancy between simulated and measurements is due to the calibration, the folded FSS does not provide a desirable response in the x-pol at a fold angle of 36.8° assuming the metric is an insertion loss greater than 10 dB. This response is expected when viewing the frequency response trend of the folding driven element simulations previously presented in Fig. 4.

5. CONCLUSION

The design, simulation, fabrication and experimental observation of an origami-inspired FSS have been demonstrated. This included a brief study of folding using driven elements to isolate the primary physical mechanisms responsible for the fold-driven polarization-dependent frequency agility. Tabulated results for center frequency, bandwidth, and percent shift upward show a correlation in performance trends for all cases examined. These results provide interest in potential applications for physical tuning as an option for shielding in fields such as robotics or space structure deployment. The geometrically defined movements of the origami-inspired FSS provide a simple and elegant solution that can be reconfigured for specific frequency filtering and shielding needs. This work has only considered the impact of folding under normal incidence, but the potential for in-service physical reconfiguratation can be inferred. Ongoing work in studying these structures at oblique incidence angles and the incorporation of new materials with new methods of fabrication will increase the abilities and manufacturability of more complex origami-inspired EM structures.

ACKNOWLEDGMENT

The authors acknowledge the support from AFOSR grant #LRIR 16RXCOR319, case number: 88ABW-2017-3814.

REFERENCES

1. Miura, K., "Method of packaging and deployment of large membranes in space," *Proceedings of 31st Congress International Astronautical Federation*, 1–10, 1980.
2. Zirbel, S. A., et al., "Accommodating thickness in origami-based deployable arrays," *Journal of Mechanical Design*, Vol. 135, No. 11, 111005, 2013.
3. Myer, J. H. and F. Cooke, "Optigami — A tool for optical systems design," *Applied Optics*, Vol. 8, No. 2, 260–260, 1969.
4. Nogi, M., N. Komoda, K. Otuska, and K. Suganuma, "Foldable nanopaper antennas for origami electronics," *Nanoscale*, Vol. 5, No. 10, 4395–4399, 2013.
5. Hayes, G. J, Y. Liu, J. Genzer, G. Lazzi, and M. D. Dickey, "Self-folding origami microstrip antennas," *IEEE Transactions on Antennas and Propagation*, Vol. 62, No. 10, 5416–5419, 2014.
6. Liu, X., S. Yao, S. V. Georgakopoulos, B. S. Cook, and M. M. Tentzeris, "Reconfigurable helical antenna based on an origami structure for wireless communication system," *2014 IEEE MTT-S International Microwave Symposium (IMS)*, 1–4, 2014.
7. Yao, S., X. Liu, J. Gibson, and S. V. Georgakopoulos, "Deployable origami Yagi loop antenna," *2015 IEEE International Symposium on Antennas and Propagation & USNC/URSI National Radio Science Meeting*, 2215–2216, 2015.
8. Yao, S., X. Liu, S. V. Georgakopoulos, and M. M. Tentzeris, "A novel reconfigurable origami spring antenna," *2014 IEEE Antennas and Propagation Society International Symposium (APSURSI)*, 374–375, 2014.
9. Fuchi, K., J. Tang, B. Crowgey, A. R. Diaz, E. J. Rothwell, and R. O. Ouedraogo, "Origami tunable frequency selective surfaces," *IEEE Antennas and Wireless Propagation Letters*, Vol. 11, 473–475, 2012.
10. Fuchi, K., et al., "Spatial tuning of a RF frequency selective surface through origami," *SPIE Defense+ Security*, 98440W–98440W-10, International Society for Optics and Photonics, 2016.
11. Demaine, E. D. and J. O'Rourke, *Geometric Folding Algorithms*, Cambridge University Press, Cambridge, 2007.
12. Lang, R. J., "Treemaker 4.0: A program for origami design," Available: http://www.langorigami.com/science/computational/ treemaker/TreeMkr40. pdf.
13. Tachi, T., "Simulation of rigid origami," *Origami*, Vol. 4, 175–187, 2009.

14. Schenk, M. and S. D. Guest, "Origami folding: A structural engineering approach," *Origami*, 291–304, 2011.
15. Fuchi, K., et al., "Origami actuator design and networking through crease topology optimization," *Journal of Mechanical Design*, Vol. 137, No. 9, 091401, 2015.
16. Fuchi, K., P. R. Buskohl, J. J. Joo, and G. W. Reich, "Control of RF transmission characteristics through origami design," *ASME International Design Engineering Technical Conference*, Charlotte, NC, 2016.
17. *High Frequency Structural Simulator*, 15th ediiton, ANSYS, Inc., Pittsburgh, PA, 2012.